Lawrence Berkeley National Laboratory

Title
Proteogenomic monitoring of Geobacter physiology during stimulated uranium bioremediation

Permalink
https://escholarship.org/uc/item/2dg4k4fw

Author
Wilkins, M.J.

Publication Date
2010-03-30

Peer reviewed

Proteogenomic monitoring of *Geobacter* physiology during stimulated uranium

bioremediation

Michael J. Wilkins[1], Nathan C. VerBerkmoes[2], Kenneth H. Williams[3], Stephen J. Callister[4], Paula J. Mouser[5], Hila Elifantz[5], A. Lucie N'Guessan[5], Brian C. Thomas[1], Carrie D. Nicora[4], Manesh B. Shah[2], Paul Abraham[2,6], Mary S. Lipton[4], Derek R. Lovley[5], Robert L. Hettich[2], Philip E. Long[7], Jillian F. Banfield[*1,3]

[1] Department of Earth and Planetary Science and Environmental Science, Policy, and Management, University of California, Berkeley, CA 94720; [2] Chemical Sciences and Biosciences Divisions, Oak Ridge National Laboratory, Oak Ridge, TN 37831; [3] Earth Science Division, Lawrence Berkeley National Laboratory, Berkeley CA 94720; [4] Biological Sciences Division, Pacific Northwest National Laboratory, Richland WA 99353; [5] Department of Microbiology, University of Massachusetts, Amherst MA 01002; [6] Graduate School of Genome Science and Technology, University of Tennessee, Knoxville, TN, 37830; [7] Energy and Environment Directorate, Pacific Northwest National Laboratory, Richland WA 99353

[*]Corresponding Author: jbanfield@berkeley.edu

Hilgard Hall, UC Berkeley, Berkeley, CA, USA, 94720

Tel: 510 643 2155

Fax: 510 643 9980

Abstract

Implementation of uranium bioremediation requires methods to monitor the membership and activities of the subsurface microbial communities that are responsible for reduction of soluble U(VI) to insoluble U(IV). Here we report a proteomics-based approach to simultaneously document strain membership and microbial physiology of the dominant *Geobacter* community members during *in situ* acetate amendment of the U-contaminated Rifle, CO aquifer. Three planktonic *Geobacter*-dominated samples were obtained from two wells down-gradient of acetate addition. Over 2,500 proteins from each of these samples were identified by matching LC MS/MS spectra to peptides predicted from 7 isolate *Geobacter* genomes. Genome-specific peptides indicate early proliferation of multiple M21 and *G. bemidjiensis*–like strains and later possible emergence of M21 and *G. bemidjiensis*–like strains more closely related to *G. lovleyi*. Throughout biostimulation, the proteome is dominated by enzymes that convert acetate to acetyl-CoA and pyruvate for central metabolism while abundant peptides matching TCA cycle proteins and ATP synthase subunits were also detected, indicating the importance of energy generation during the period of rapid growth following the start of biostimulation. Evolving *Geobacter* strain composition may be linked to changes in protein abundance over the course of biostimulation and may reflect changes in metabolic functioning. Thus, metagenomics-independent community proteogenomics can be used to diagnose the status of the subsurface consortia upon which remediation biotechnology relies.

Introduction

Enzymatic reduction of U(VI) to insoluble U(IV) by dissimilatory Fe(III)-reducing bacteria (DIRB) can limit subsurface U(VI) migration (2, 20, 21). This observation provided the basis for an important new biotechnology that involves remediation of contaminated groundwater by organic amendment-based stimulation of the activities of DIRB. Despite the obvious high potential value, there are significant technological challenges that must be overcome before this approach can be deployed as a functional biotechnology. *In situ* U(VI) reduction rates are directly coupled to microbial physiology and community composition, both of which change as bioremediation progresses (23, 25, 29). Thus, a key need is the ability to monitor changes in microbial community membership and function as they occur, so that optimal management strategies can be implemented to achieve the desired geochemical outcomes. This challenge is significant because metal reduction occurs within pore spaces deep in the aquifer and the process is associated with vast numbers of microbial cells distributed in the subsurface.

Changes in the complements of DIRB proteins should reflect shifts in microbial physiology and could be used to monitor in situ bioremediation technologies if microbial proteomes could be tracked during organic amendment. Proteomic methods have been used previously to detect physiological responses of microorganisms growing in pure culture (8, 17, 18) and in genomically characterized natural microbial communities (7, 19, 27, 35). Strain-resolved proteomic approaches (19) have the potential to also track changes in microbial community composition. Previously, the use of proteomic analysis techniques to monitor subsurface

bioremediation has been precluded by the lack of metagenomic data. Here we used seven isolate *Geobacter* genomes to generate a reference database against which peptide data measured using liquid chromatography-based high-resolution tandem mass spectrometry (2D-LC-MS/MS) were compared for protein identification. Although differences between environmental and isolate peptide sequences may preclude peptide identification, peptides common to multiple *Geobacter* types and isolates enable protein identification and peptides unique to one isolate constrain environmental genotypes. Simultaneous analysis of community structure and function in natural microbial communities that relies upon proteomics-derived genomic insights is referred to as proteogenomics (Fig. 1). In the current study, a proteogenomic approach was applied to monitor the progress of an *in situ* U-bioremediation project carried out at the DOE Integrated Field Research Challenge (IFRC) site in Rifle, Colorado. Despite strain complexity in the recovered samples, proteomic data provided insights into the community structure and physiology of planktonic *Geobacter* in aquifer solutions as groundwater U(VI) concentrations decreased.

Materials and Methods

Injection gallery design and operation. The Winchester field experiment was carried out during August and September 2007 (8th August – 12th September) at the Rifle IFRC site in Western Colorado where groundwater U concentrations are typically ~ 1 μM. An injection gallery consisting of 10 injection wells, 12 down-gradient monitoring wells arranged in three rows, and three up-gradient monitoring wells was constructed using sonic rotary drilling (Fig. S1). Acetate:bromide (50 mM:5 mM) amended groundwater was injected into the subsurface to provide a target acetate concentration of ~ 5 mM which acted as electron donor over the course of the amendment experiment. Geochemical samples were taken from 17 ft depth after purging 12 L groundwater, and were analyzed in the field and at Lawrence Berkeley National Laboratory. Ferrous iron and sulfide concentrations were analyzed immediately following sampling using the HACH phenanthroline assay and sulfide reagent kit respectively (HACH, CO, USA). Acetate was analyzed using a Dionex ICS1000 ion chromatograph equipped with a CD25 conductivity detector and a Dionex IonPac AS22 column (Dionex, CA, USA). U(VI) values were determined using a Kinetic Phosphorescence Analyzer (KPA) (Chemchek, WA, USA) at the DOE Grand Junction office.

Sample collection. Three biomass samples were recovered from groundwater over the course of the *in situ* bioreduction experiment. Two samples were taken from well D07 and one from well D05, both wells being located in the second row of down-gradient monitoring wells. For each sample 500 L of groundwater pumped at approximately 2 l min^{-1} from a well was filtered

through a pre-filter (1.4 μm, 292 mm diameter Supor disc filter, Pall Corporation, NY, USA), followed by a Pelicon tangential flow filtration system (0.2 μm) (Millipore, MA, USA) to concentrate biomass. Groundwater was passed through a series of chilling baths containing an ice/rock salt mixture as soon as it was pumped to the surface to minimize changes to the proteome. Chilling baths ensured that the groundwater temperature was approximately 1 ^{o}C as it passed through the filtration system which was located in an air-conditioned trailer. Biomass was concentrated to ~ 200 ml in the retentate vessel and centrifuged at 4,000 rpm for 40 minutes at 4 ^{o}C. The resulting pellet was resuspended in ~ 5 ml of groundwater, immediately frozen in an ethanol-dry ice mix, and shipped overnight on dry ice to Oak Ridge National Laboratory and Pacific Northwest National Laboratory for proteomic analysis.

Proteomics

In order to ensure that the proteomic analyses were as robust as possible, all experiments were conducted in two different laboratories using parallel but distinct procedures and instrumentation. Results from both laboratories are provided in Table S2. Values with Normalized Spectral Abundance Frequency (NSAF) scores (see below for details) below 1 x 10^{-5} were removed and values between this and 1 x 10^{-4} are shown in grey text. Despite many opportunities for discrepancies, the data indicate good replication and all conclusions are based on patterns evident in both datasets. Plots in the manuscript are generated from ORNL data.

ORNL Shotgun proteomics via 2D-LC-MS/MS. Cells in ~500 uL of sample were lysed in a single tube and processed using a method optimized for small samples in which the proteins were denatured, reduced, and digested with sequencing grade Trypsin (33). Approximately 1/5 of

each digested sample was used for each of three technical replicates for the three samples. Samples were analyzed via 22-hour two-dimensional (2D) nano-LC MS/MS with a split-phase column (RP-SCX-RP) on a hybrid linear ion trap-Orbitrap mass spectrometer (Thermo Fisher Scientific, MA, USA), as previously described (35). The linear ion trap (LTQ) and Orbitrap settings were as follows: 30K resolution on full scans in Orbitrap, all data-dependent MS/MS in LTQ (top five), 2 microscans for both full and MS/MS scans, with centroid data for all scans and 2 microscans averaged for each spectra with the dynamic exclusion set at 1.

All samples and technical replicates were searched against two databases, the first contained 862 isolate genomes with ~3 million proteins entries (http//img.jgi.doe.gov/) plus a *Geobacter* sub-database that contained ~26,000 Geobacter proteins (from seven species). Common contaminants such as Trypsin and keratin were included in both databases. All MS/MS spectra were searched against both databases with the SEQUEST algorithm (11) and filtered with DTASelect/Contrast (31) at the peptide level with conservative filters [Xcorrs of at least 1.8 (+1), 2.5 (+2) 3.5 (+3)]. Only proteins identified with two fully tryptic peptides at conservative filter levels were considered for further analysis.

We applied the accepted method of reverse database searching to determine false positive levels on a subset of the data with the filters given above (26) (9). This reverse database searching method was designed and tested with single yeast genomes and proteomes. For the proteomics analysis presented here the very large percentage of non-unique peptides (often the case in metaproteomics-type experiments), and the unknown degree of genomic sequence representation to the samples make the accuracy of false positive level estimation

questionable. Nevertheless, we attempted this established method and calculated the false positive levels twice, once with only unique peptides, and once with all peptides. With unique peptides, the false positive rate was between 5-8% which is overestimated due to the massive reduction in real peptides that have non-unique status. With all the peptides considered, the rate falls to 0.6-0.9%, which is underestimated due to the addition of many non-unique peptides when truly only one peptide existed (up to seven maximum, the number of *Geobacter* species in the database). Since both datasets were then filtered again during the comparison stage to remove all proteins with very low NSAF values it can be assumed that the final list used for biological analyses had a very low false discovery rate. All databases, peptide and protein results, MS/MS spectra and supplementary tables for all database searches from the ORNL dataset are archived and made available as open access via:

http://compbio.ornl.gov/ersp_rifle/ground_water_2007

PNNL proteomics via LC-tandem mass spectrometry and peptide putative mass and elution time tag assignments. Global as well as soluble, and insoluble protein fractions were extracted from cell pellets using established protocols (1, 18). Briefly, frozen cells were thawed on ice, washed using 100 mM NH4HCO3, pH 8.4 buffer, and then suspended in a new aliquot of this buffer. Cells were lysed via Pressure Cycling Technology (PCT) using a barocycler (Pressure BioSciences Inc., South Easton, MA). The suspended cells were subjected to 20 seconds of high pressure at 35 kpsi followed by 10 seconds of ambient pressure for 10 cycles. The protein concentration was determined by a Coomassie assay (Thermo Scientific, Rockford, IL). Protein extraction, digestion and HPLC fractionation were performed as previously described (4). From

each collected fraction, peptides were analyzed by reversed phase HPLC separation coupled to an LTQ ion trap mass spectrometer (ThermoFisher Scientific Corp., San Jose, CA) operated in a data-dependent MS/MS mode. Acquired spectra from approximately ~400 MS/MS experiments were analyzed using the SEQUEST algorithm (11) in conjunction with predicted protein annotations concatenated from the 7 *Geobacter* genomes Sequest results were preliminarily filtered (XCorr >= 1.9, 2.2, or 3.5 for 1+, 2+, or >=3+ if seen once, XCorr >= 1.9 if seen >= 2 times, no cleavage rules, min. length 6), extracted, and processed using the PRISM proteomics pipeline developed in-house (16).

Peptide mapping and strain variant analysis. Probable orthologous proteins were identified by BLASTP (http://blast.ncbi.nlm.nih.gov/Blast.cgi) searches between predicted proteins from the seven *Geobacter* isolates as proteins exhibiting 30% amino acid similarity over 70% of the alignment length (6, 28). Tables showing distribution across the seven *Geobacter* species were constructed as previously described (5). Spectral count data was normalized using the Normalized Spectral Abundance Frequency (NSAF) technique (37) and averaged over three technical replications per sample for the ORNL dataset. While this technique was initially developed for analysis of isotope-labeled data, the statistical basis of the method allows for the normalization of data to account for biases arising from protein length in this instance. Peptides were mapped onto alignments of inferred orthologous proteins using an in house script which at a protein-by-protein level, allows simultaneous visualization of unique (in single isolate genomes) and non-unique (shared by one or more genomes) peptides as well as spectral count information. Within this program, identified peptides are rendered for individual samples, technical replicate runs, and for multiple samples.

Results

U(VI) groundwater concentrations were elevated at the time of collection of the D07(1) and D05 samples (~ 0.7 and 1.4 μM respectively), and lower (~ 0.1 μM) when D07(2) was collected (Fig. 2). D07(1) and D05 were collected during the early phase of iron reduction and D07(2) later in iron reduction.

Following protein extraction from the samples and 2D-LC MS/MS (see methods), tandem mass spectra from all samples were searched against a database containing 862 isolate genomes (http//img.jgi.doe.gov/). Approximately 95% of all unique peptides identified matched *Geobacter* proteins, indicating that all samples were dominated by *Geobacter* species. The majority of the remaining unique peptides matched closely related microorganisms such as *Pelobacter* species (13) (see Supplementary Materials). Subsequently, proteomic data were searched against a database (Supplementary Materials) of predicted peptides from seven *Geobacter* isolate genomes: *G. bemidjeisis, G. metallireducens, G. sulfurreducens* PCA*, G. lovleyi* SZ*, G. uraniireducens* Rf4, strain FRC-32 and strain M21. Between 2,000 - 2,500 proteins identified in each sample using these sub-database searches were then used in subsequent biological analyses (see Methods). While only three samples were collected, differences in proteomic patterns suggest some interesting changes in microbial community structure and activity.

Strain composition. Mass spectra counts for spectra unique to each isolate *Geobacter* species in each sample were quantified (Fig. 3A) using a database with only the six *Geobacter* species that share between ~ 60-70 % amino acid similarity across the 1,480 to 2,291 homologous

proteins (*G. bemidjiensis, G. sulfurreducens, G. metallireducens, G. uraniireducens, G. lovleyi* and *Geobacter* strain FRC-32,* see Table S1). Unique spectral counts show that a strain or strains closely related to *G. bemidjiensis* dominated (60-70%) all three samples. Strain M21 was excluded from this initial analysis because the 3,098 proteins homologous with *G. bemidjiensis* share ~ 95 % average amino acid identity (Table S1). Addition of the strain M21 genome would lead to classification of peptides shared with *G. bemidjiensis* as non-unique, prohibiting their inclusion in unique spectral counts for both strains. However, inclusion of strain M21 in the protein database for all subsequent analyses increased our ability to identify peptides and allowed higher resolution analysis of strain makeup and activity.

While unique spectra for all *Geobacter* isolates were detected in all samples, each sample could, in principle, contain only one genotype. This "hypothetical" genotype would encode peptides classified as unique to each of all seven isolates. Thus, determination of strain makeup requires proteome-wide analysis of coexisting unique peptides of all seven *Geobacter* genotypes (see Fig. 1). The identification of multiple homologous peptides that differ in their amino acid sequences indicates the presence of multiple genotypes. It is also possible to profile strain composition based on the numbers of peptides characteristic of each isolate genotype.

 In D07(2) compared to D07(1), the fraction of unique spectra matching *G. lovleyi* increased from ~4% to ~15% (Fig. 3B). Proteogenomic inference of the strain composition of the community in the D07(2) sample is indicated in Figure 3C. The figure illustrates the relative even distribution along the genome of unique peptides matching *G. bemidjiensis*, but the presence of unique peptides characteristic of *G. lovleyi* at a few loci, implying that the actual

genotype has amino acid sequence similarity to *G. lovleyi* at these loci. Thus, late in iron reduction (D07(2)), we infer the proliferation of a strain or strains whose genotype remains most closely related to *G. bemidjiensis* – strain M21, but which has an increased fraction of loci shared with *G. lovleyi*, or increased activity of such a strain(s).

Mapping of peptides onto alignments of homologous proteins predicted from the 7 isolate genomes revealed that the best coverage of protein sequences by identified peptides was generally achieved by non-unique plus unique peptides of strain M21 and/or *G. bemidjiensis*. Over the entire proteomic dataset, the combination of sequence coverage and spectral count data indicates dominance by a strain or strains slightly more closely related to M21 (isolated from the Rifle, CO site) than *G. bemidjiensis*. The coexistence of multiple strain variants in the Rifle subsurface under biostimulated conditions is indicated by the simultaneous identification of unique spectra from homologous peptides (see example in Figs. 4 and S3).

Microbial metabolism. Relative protein abundances, inferred from numbers of spectral counts per protein (see methods), indicate intriguing shifts in specific functional classes over the sampling period (Fig. 5). Rapid growth and protein production under biostimulated conditions was reflected in the abundance of detected peptides matching chemotaxis (see supplemental info.) and ribosomal proteins (36), while spectra matching ATP synthase F1 subunit proteins in all samples indicate the high energy demand of *Geobacter* species associated with this growth. However, these proteins, together with proteins associated with nutrient stress (metal efflux, P acquisition) were inferred to be more abundant in D07(1) than D07(2), suggestive of a slowing growth rate later in Fe(III) reduction. Corresponding abundance increases from D07(1) to

D07(2) for several TCA cycle proteins (citrate synthase, isocitrate dehydrogenase) and the acetate-activating enzyme acetyl-CoA hydrolase (Fig. 5) suggest a shift in *Geobacter* energy metabolism, possibly tied to changes in strain makeup and slowing growth rates.

Increases in the abundance of citrate synthase, responsible for controlling flux into the TCA cycle by catalyzing the condensation of acetyl-CoA and oxaloacetate to citric acid (3), corresponded to the identification of more *G. lovleyi* and *G. uraniireducens* unique spectra (10- to 20- fold increases). However, spectral count data for conserved peptides confirm that the inferred increase was not simply due to a shift in strain type towards the genomically-characterized isolates. There are more than twice as many spectral counts for a conserved peptide shared by all genotypes that contains a citrate binding site detected in D07(2) relative to D07(1). The identification of co-existing homologous unique peptides associated with this protein indicates at least four *Geobacter* strain variants in D07(2) (Fig. S3). Similar patterns were observed for unique peptides matching isocitrate dehydrogenase as the period of biostimulation increased. Increases in unique spectra in D07(2) relative to D07(1) (seven-fold for unique spectra matching *G. lovleyi*) were again suggestive of a shift towards strains related to *G. lovleyi* and *G. uraniireducens*, while there was a concurrent doubling of spectra matching a highly conserved peptide present in all isocitrate dehydrogenase variants.

As expected during acetate biostimulation, peptides of acetyl-CoA hydrolase, which catalyzes the activation of acetate to acetyl-CoA for use in the TCA cycle, were highly detected in all three samples. An additional pathway for acetyl-CoA formation via acetate kinase and phosphotransacetylase was evident from the proteomic data, although lower spectral counts

for this compared to the acetyl-CoA hydrolase pathway may indicate that this was not the primary mechanism for acetyl-CoA formation. Peptides matching succinyl-CoA synthetase from M21 - *G. bemidjiensis*-like strains were identified, indicating the potential for operation of a complete TCA cycle in these organisms without acetyl-CoA transferase activity (30) (Fig. 6).

Detected at similarly high abundance to acetyl-CoA hydrolase in all samples were peptides of pyruvate ferredoxin oxioreductase (Por), which plays a key role in 3-carbon synthesis from acetyl-CoA in *Geobacter* (22). Pyruvate metabolism opens an additional pathway for acetate utilization, with pyruvate carboxylase, pyruvate phosphate dikinase, and phosphoenolpyruvate carboxykinase all identified by proteomics from M21 and *G. bemidjiensis*-like strains. These enzymes convert pyruvate to oxaloacetate, which can enter the TCA cycle (Fig. 6) (34).

Discussion

The proteomic analysis of three microbial planktonic samples here allows the identification of a range of important pathways utilized by *Geobacter* sp. in the subsurface during biostimulation, and suggests possible ways that the community may evolve during the process. Intriguing shifts in the abundance of certain protein groups are also suggested by the data. Results indicate dominance of *Geobacter* strains from "Subsurface Clade I" (15) during the first 20 days of acetate amendment, the presence of multiple coexisting active strain variants, and high abundance of proteins involved in the efficient utilization of acetate (14). Acetyl-CoA hydrolase enables *Geobacter* to utilize acetate and we infer that this is the primary route by which the subsurface community creates acetyl-CoA for energy (TCA cycle) and biomass production. In

14

addition, acetate kinase and phosphtransacetylase offer another pathway for acetyl-CoA synthesis. All TCA cycle proteins were identified by proteomics, including succinyl-CoA synthetase from M21 and *G. bemidjiensis*-like strains. Given the absence of succinyl-CoA synthetase activity in *G. sulfurreducens,* the acetate kinase-phosphtransacetylase pathway was recently described as the mechanism by which this organism produces acetyl-CoA for biomass production (30). It also has been suggested that in *G. metallireducens*, acetyl-CoA accumulation forces the transformation of succinate to succinyl-CoA, limiting the rate of carbon metabolism through the TCA cycle (32). If correct, these observations may explain the slow growth of *G. metallireducens*- and possibly *G. sulfurreducens*-like strains in these acetate-amended communities and the dominance of M21 and *G. bemidjiensis*-like strains.

Another important observation is the high abundance of Por, which may enable *Geobacter* to "fix" some additional carbon by combining acetyl-CoA and carbon dioxide to form pyruvate (12). Modeling calculations suggest that this pathway allows *G. sulfurreducens* to synthesize amino acids more efficiently than *Escherichia coli* (22). While this enzyme also catalyzes the oxidative decarboxylation of pyruvate to acetate and CO_2, given the non-limiting carbon concentrations (10), the potential high activity of the pyruvate synthase pathway may be an important response of M21 and *G. bemidjiensis*-like strains to high acetyl-CoA availability during acetate amendment.

It is important to note that our perspective on changes in subsurface microbial activity is limited to planktonic cells. *Geobacter* require direct access to ferric iron-bearing minerals (24), including ferric iron-bearing clays and oxyhydroxide minerals that are readily dispersed during

drilling activities and well installation. As a result, Fe(III)-bearing phases of small particle size and hence large specific surface area are concentrated in the vicinity of well bores in advance of acetate amendment. The fraction of bioavailable minerals that are readily accessible to planktonic cells declines over time due to enzymatic reductive dissolution and settling. Thus, it is not surprising that the acetate-stimulated *Geobacter* bloom is associated with a higher initial investment in proteins required for active growth (ribosomal proteins) (36) and nutrient acquisition. While slowing cell growth (suggested by decreasing abundances of ribosomal proteins and ATP synthase subunits in D07(2)) might be expected later in biostimulation as concentrations of electron acceptors and nutrients drop, the corresponding increases in TCA cycle proteins may indicate a shift in energy investment. Many of these abundance increases were associated with increases in unique spectra matching *G. loveyi*, suggesting a potential shift in strain composition towards *Geobacter* that are still closely related to *G. bemidjiensis* and strain M21, but with some similarity to *G. lovleyi*. Understanding exactly how these changes in metabolic function and strain composition are linked to geochemical parameters will require the analysis of additional biomass samples to conclusively demonstrate these trends.

The current study is the first to use isolate genome sequences to enable extensive mass spectrometry-based proteomic analysis of natural microbial communities. There is no question that more peptides and proteins would be identified had metagenomic data for these samples been available. Despite the limitations of the isolate sequence-based approach, over 13,000 peptides and 2,500 proteins were identified from each sample. Identification of each peptide confirmed the presence of that sequence in the sample and each protein contributed to a rendering of the physiological state of *Geobacter* strains in the communities. As currently

deployed, proteogenomics is a complicated approach that depends on sophisticated technological methods. However, by analogy with medical diagnostics, it is reasonable to anticipate that rapid, high throughput methods can be developed to detect signals characteristic of the metabolic state of microbial communities in the subsurface and elsewhere.

References

1.   **Adkins, J. N., H. M. Mottaz, A. D. Norbeck, J. K. Gustin, J. Rue, T. R. W. Clauss, S. O. Purvine, K. D. Rodland, F. Heffron, and R. D. Smith.** 2006. Analysis of the *Salmonella typhimurium* proteome through environmental response toward infectious conditions. Mol. Cell. Prot. **5:**1450-1461.

2.   **Anderson, R. T., H. A. Vrionis, I. Ortiz-Bernad, C. T. Resch, P. E. Long, R. Dayvault, K. Karp, S. Marutzky, D. R. Metzler, A. Peacock, D. C. White, M. Lowe, and D. R. Lovley.** 2003. Stimulating the in situ activity of *Geobacter* species to remove uranium from the groundwater of a uranium-contaminated aquifer. Appl. Environ. Microbiol. **69:**5884-5891.

3.   **Bond, D. R., T. Mester, C. L. Nesbo, A. V. Izquierdo-Lopez, F. L. Collart, and D. R. Lovley.** 2005. Characterization of citrate synthase from *Geobacter sulfurreducens* and evidence for a family of citrate synthases similar to those of eukaryotes throughout the *Geobacteraceae*. Appl. Environ. Microbiol. **71:**3858-3865.

4.   **Callister, S. J., M. A. Dominguez, C. D. Nicora, X. Zeng, C. L. Tavano, S. Kaplan, T. J. Donohue, R. D. Smith, and M. S. Lipton.** 2006. Application of the accurate mass and time tag approach to the proteome analysis of sub-cellular fractions obtained from

Rhodobacter sphaeroides 2.4.1. Aerobic and photosynthetic cell cultures. J. Proteome Res. **5:**1940-1947.

5. **Callister, S. J., L. A. McCue, J. E. Turse, M. E. Monroe, K. J. Auberry, R. D. Smith, J. N. Adkins, and M. S. Lipton.** 2008. Comparative bacterial proteomics: Analysis of the core genome concept. PLoS ONE **3:**e1542.

6. **Chain, P. S. G., V. J. Denef, K. T. Konstantinidis, L. M. Vergez, L. Agullo, V. L. Reyes, L. Hauser, M. Cordova, L. Gomez, M. Gonzalez, M. Land, V. Lao, F. Larimer, J. J. Lipuma, E. Mahenthiralingam, S. A. Malfatti, C. J. Marx, J. J. Parnell, A. Ramette, P. Richardson, M. Seeger, D. Smith, T. Spilker, W. J. Sul, T. V. Tsoi, L. E. Ulrich, I. B. Zhulin, and J. M. Tiedje.** 2006. *Burkholderia xenovorans* LB400 harbors a multi-replicon, 9.73-Mbp genome shaped for versatility. Proc. Natl. Acad. Sci. USA. **103:**15280-15287.

7. **Denef, V. J., M. B. Shah, N. C. VerBerkmoes, R. L. Hettich, and J. F. Banfield.** 2007. Implications of strain- and species-level sequence divergence for community and isolate shotgun proteomic analysis. J. Proteome Res. **6:**3152-3161.

8. **Ding, Y. H. R., K. K. Hixson, C. S. Giometti, A. Stanley, A. Esteve-Nunez, T. Khare, S. L. Tollaksen, W. H. Zhu, J. N. Adkins, M. S. Lipton, R. D. Smith, T. Mester, and D. R. Lovley.** 2006. The proteome of dissimilatory metal-reducing microorganism *Geobacter sulfurreducens* under various growth conditions. BBA-Proteins Proteom. **1764:**1198-1206.

9. **Elias, J. E., and S. P. Gygi.** 2007. Target-decoy search strategy for increased confidence in large-scale protein identification by mass spectrometry. Nature Methods **4:**207-214.

10. **Elifantz, H., L. A. N'Guessan, P. J. Mouser, K. H. Williams, M. J. Wilkins, J. E. Ward, P. E. Long, and D. R. Lovley** 2008. Presented at the Abstracts: American Society for Microbiology 108th General Meeting, Boston, MA.

11. **Eng, J. K., A. L. McCormack, and J. R. Yates III.** 1994. An approach to correlate tandem mass spectral data of peptides with amino acid sequences in a protein database. J. Am. Soc. Mass Spectr. **5:**976-989.

12. **Furdui, C., and S. W. Ragsdale.** 2000. The role of pyruvate ferredoxin oxidoreductase in pyruvate synthesis during autotrophic growth by the Wood-Ljungdahl pathway. J. Biol. Chem. **275:**28494-28499.

13. **Holmes, D. E., K. P. Nevin, and D. R. Lovley.** 2004. Comparison of 16S rRNA, nifD, recA, gyrB, rpoB and fusA genes within the family *Geobacteraceae* fam. nov. Int. J. Syst. Evol. Microbiol. **54:**1591-1599.

14. **Holmes, D. E., K. P. Nevin, R. A. O'Neil, J. E. Ward, L. A. Adams, T. L. Woodard, H. A. Vrionis, and D. R. Lovley.** 2005. Potential for quantifying expression of the *Geobacteraceae* citrate synthase gene to assess the activity of *Geobacteraceae* in the subsurface and on current-harvesting electrodes. Appl. Environ. Microbiol. **71:**6870-6877.

15. **Holmes, D. E., R. A. O'Neil, H. A. Vrionis, L. A. N'Guessan, I. Ortiz-Bernad, M. J. Larrahondo, L. A. Adams, J. A. Ward, J. S. Nicoll, K. P. Nevin, M. A. Chavan, J. P. Johnson, P. E. Long, and D. R. Lovley.** 2007. Subsurface clade of *Geobacteraceae* that predominates in a diversity of Fe(III)-reducing subsurface environments. ISME J. **1:**663-677.

16. **Kiebel, G. R., K. J. Auberry, N. Jaitly, D. A. Clark, M. E. Monroe, E. S. Peterson, N. Tolic, G. A. Anderson, and R. D. Smith.** 2006. PRISM: A data management system for high-throughput proteomics. Proteomics **6:**1783-1790.

17. **Kolker, E., A. F. Picone, M. Y. Galperin, M. F. Romine, R. Higdon, K. S. Makarova, N. Kolker, G. A. Anderson, X. Y. Qiu, K. J. Auberry, G. Babnigg, A. S. Beliaev, P. Edlefsen, D. A. Elias, Y. A. Gorby, T. Holzman, J. A. Klappenbach, K. T. Konstantinidis, M. L. Land, M. S. Lipton, L. A. McCue, M. Monroe, L. Pasa-Tolic, G. Pinchuk, S. Purvine, M. H. Serres, S. Tsapin, B. A. Zakrajsek, J. H. Zhou, F. W. Larimer, C. E. Lawrence, M. Riley, F. R. Collart, J. R. Yates, R. D. Smith, C. S. Giometti, K. H. Nealson, J. K. Fredrickson, and J. M. Tiedje.** 2005. Global profiling of *Shewanella oneidensis* MR-1: Expression of hypothetical genes and improved functional annotations. Proc. Natl. Acad. Sci. USA. **102:**2099-2104.

18. **Lipton, M. S., L. Pasa-Tolic, G. A. Anderson, D. J. Anderson, D. L. Auberry, K. R. Battista, M. J. Daly, J. Fredrickson, K. K. Hixson, H. Kostandarithes, C. Masselon, L. M. Markillie, R. J. Moore, M. F. Romine, Y. F. Shen, E. Stritmatter, N. Tolic, H. R. Udseth, A. Venkateswaran, L. K. Wong, R. Zhao, and R. D. Smith.** 2002. Global analysis of the *Deinococcus radiodurans* proteome by using accurate mass tags. Proc. Natl. Acad. Sci. USA. **99:**11049-11054.

19. **Lo, I., V. J. Denef, N. C. VerBerkmoes, M. B. Shah, D. Goltsman, G. DiBartolo, G. W. Tyson, E. E. Allen, R. J. Ram, J. C. Detter, P. Richardson, M. P. Thelen, R. L. Hettich, and J. F. Banfield.** 2007. Strain-resolved community proteomics reveals recombining genomes of acidophilic bacteria. Nature **446:**537-541.

20.   **Lovley, D. R., and E. J. P. Phillips.** 1992. Bioremediation of uranium contamination with enzymatic uranium reduction. Environ. Sci. Technol. **26:**2228-2234.

21.   **Lovley, D. R., E. J. P. Phillips, Y. A. Gorby, and E. Landa.** 1991. Microbial reduction of uranium. Nature **350:**413-416.

22.   **Mahadevan, R., D. R. Bond, J. E. Butler, A. Esteve-Nunez, M. V. Coppi, B. O. Palsson, C. H. Schilling, and D. R. Lovley.** 2006. Characterization of metabolism in the Fe(III)-reducing organism *Geobacter sulfurreducens* by constraint-based modeling. Appl. Environ. Microbiol. **72:**1558-1568.

23.   **Mouser, P. J., L. A. N'Guessan, H. Elifantz, D. E. Holmes, K. H. Williams, M. J. Wilkins, P. E. Long, and D. R. Lovley** 2008. Impact of heterogeneous ammonium availability on community structure and the expression of nitrogen fixation and ammonium transporter genes during *in situ* bioremediation of uranium-contaminated groundwater. Environ. Sci. Technol. **43:**4386-4392

24.   **Nevin, K. P., and D. R. Lovley.** 2000. Lack of production of electron-shuttling compounds or solubilization of Fe(III) during reduction of insoluble Fe(III) oxide by *Geobacter metallireducens*. Appl. Environ. Microbiol. **66:**2248-2251.

25.   **North, N. N., S. L. Dollhopf, L. Petrie, J. D. Istok, D. L. Balkwill, and J. E. Kostka.** 2004. Change in bacterial community structure during *in situ* biostimulation of subsurface sediment co-contaminated with uranium and nitrate. Appl. Environ. Microbiol. **70:**4911-4920.

26. **Peng, J., J. E. Elias, C. C. Thoreen, L. J. Licklider, and S. P. Gygi.** 2003. Evaluation of multidimensional chromatography coupled with tandem mass spectrometry (LC/LC-MS/MS) for large-scale protein analysis: the yeast proteome. J. Proteome Res. **2:**43-50.

27. **Ram, R. J., N. C. VerBerkmoes, M. P. Thelen, G. W. Tyson, B. J. Baker, R. C. Blake, M. Shah, R. L. Hettich, and J. F. Banfield.** 2005. Community proteomics of a natural microbial biofilm. Science **308:**1915-1920.

28. **Rasko, D. A., G. S. A. Myers, and J. Ravel.** 2005. Visualization of comparative genomic analyses by BLAST score ratio. BMC Bioinformatics **6**.2

29. **Scheibe, T. D., R. Mahadevan, Y. Fang, S. Garg, P. E. Long, and D. R. Lovley** 2009. Coupling a genome-scale metabolic model with a reactive transport model to describe *in situ* uranium bioremediation. Microbial Biotechnology **2:**274-286.

30. **Segura, D., R. Mahadevan, K. Juarez, and D. R. Lovley.** 2008. Computational and experimental analysis of redundancy in the central metabolism of *Geobacter sulfurreducens*. PloS Comput. Bio. **4**.e36

31. **Tabb, D. L., W. H. McDonald, and J. R. Yates III.** 2002. DTASelect and Contrast: Tools for assembling and comparing protein identifications from shotgun proteomics. J. Proteome Res. **1:**21-26.

32. **Tang, Y. J. J., R. Chakraborty, H. G. Martin, J. Chu, T. C. Hazen, and J. D. Keasling.** 2007. Flux analysis of central metabolic pathways in *Geobacter metallireducens* during reduction of soluble Fe(III)-nitrilotriacetic acid. Appl. Environ. Microbiol. **73:**3859-3864.

33. **Thompson, M. R., K. Chourey, J. M. Froelich, B. K. Erickson, N. C. VerBerkmoes, and R. L. Hettich.** 2008. Experimental approach for deep proteome measurements from small-scale microbial biomass samples. Anal. Chem. **80:**9517-9525.

34. **Utter, M. F., and D. B. Keech.** 1960. Formation of oxaloacetate from pyruvate and carbon dioxide. J. Biol. Chem. **235:**17-18.

35. **VerBerkmoes, N. C., A. L. Russell, M. Shah, A. Godzik, M. Rosenquist, J. Halfvarson, M. G. Lefsrud, J. Apajalahti, C. Tysk, R. L. Hettich, and J. K. Jansson.** 2008. Shotgun metaproteomics of the human distal gut microbiota. ISME J. **3:**179-189

36. **Xiao, L. J., and A. Grove.** 2009. Coordination of ribosomal protein and ribosomal RNA gene expression in response to TOR signaling. Curr. Genom. **10:**198-205.

37. **Zybailov, B., A. L. Mosley, M. E. Sardiu, M. K. Coleman, L. Florens, and M. P. Washburn.** 2006. Statistical analysis of membrane proteome expression changes in *Saccharomyces cerevisiae*. J. Proteome Res. **5:**2339-2347.

Figure Legends

Figure 1. Strain-resolved proteogenomic techniques allow identification of unique peptides and constrain the genotypes present in environmental samples. (1) Proteins were predicted from the seven isolate *Geobacter* genomes. (2) Proteins were aligned. In the example shown, they share a conserved region (similar colors in all seven regions) and have a variable region (indicated by the variety of colors for each protein). (3) Tryptic digest patterns are used to predict peptide sequences. (4) Proteins were extracted from the experimental sample and (5) digested into peptides using Trypsin. (6) These peptides were separated using liquid chromatography before (7) high-resolution mass spectrometry on a fraction of peptides from an elution peak to determine the mass of the parent ions. (8) The peptides are fragmented and mass spectrometry measurements made on fragment ions. (9) Mass spectral data are matched to peptide sequences predicted in step (3) to allow peptide identification. Peptide sequences differing by only one amino acid can be identified, as shown in the spectra diagram. (10) Detected peptides are mapped onto aligned protein sequences to identify peptides shared or unique to each of the isolate species. Spectral counts can be mapped together with peptides. Where co-existing unique peptides are detected, ratios of unique spectral counts can be used to infer relative strain abundance. As shown, the identification of a unique peptide indicates that this protein is most closely related to that of *G. bemidjiensis*.

Figure 2. Acetate, Fe(II) and U(VI) geochemical data for the two proteomic sampling wells (D05 & D07) over the time-course of the biostimulation experiment. The grey dashed line indicates

the start of acetate amendment, whereas the full grey lines denote a proteomic sampling event.

Figure 3. Counts of spectra unique to the *Geobacter* isolates as a percentage of the total number of unique spectra per sample. (3a) Unique spectral count data when experimental results were searched using only the six *Geobacter* species with ~ 60-70% amino acid identity (Strain M21 excluded). (3b) Spectral count patterns generated by a database search consisting of all seven *Geobacter* isolates (i.e., the Strain M21 is included). The percentage of spectra unique to *G. bemidjiensis* drops greatly when strain M21 is included due to the high amino acid sequence identity between G*. bemidjiensis* and strain M21. (3c) Unique spectral counts for *G. bemidjiensis* and *G. lovleyi* in D07(2) plotted as a function of gene order. There are several loci where increased detection of unique spectra matching *G. lovleyi* indicates an environmental strain with similarity to both *G. bemidjiensis* and *G. lovleyi*.

Figure 4. Identified peptide data from sample D07(1) mapped onto a schematic of aligned ribosomal S9 proteins. This data illustrates how inferences about strain makeup are achieved. Red regions indicate non-unique peptides and blue regions indicate unique peptides. Expanded sections show the aligned amino acid sequence, with values displaying spectral counts for each peptide. Unique homologous *G. metallireducens, G. uraniireducens,* and *G. bemidjiensis* peptides and peptides unique to the *G. bemidjiensis* - strain M21 group were present (regions **a** and **b**). The unique *G. metallireducens* peptide was identified much less frequently than the homologous *G. bemidjiensis* and strain M21 peptide (1 vs. 14 spectral counts), suggesting the presence of a second protein variant at low abundance. Conversely, the unique *G. bemidjiensis*

- strain M21 and *G. uraniireducens* peptides have comparable spectral counts (7 vs. 9 spectral counts), consistent with two relatively equally abundant strain variants. The highest coverage is obtained using the *G. bemidjiensis* sequence due to the identification of a unique *G. bemidjiensis* peptide (section **c**). Given this, and the high spectral count for this peptide, we infer that the dominant S9 ribosomal protein is from an organism more closely related to *G. bemidjiensis* than to other *Geobacter* isolates.

Figure 5. Changes in abundance of protein functional categories between early and late Fe(III) reduction samples based on the ratio between NSAF values in D07(1) and D07(2). The patterns indicate a shift from a period of initial rapid growth to slower growth coupled to increasing energy demand later during biostimulation.

Figure 6. *Geobacter* central metabolism elucidated using identified peptides. Arrow thicknesses indicate relative abundances based on spectral count data for each protein.

2-Ims, 2-isopropylmalate synthase; Ack, Accetate kinase; Acs, Acetolactate synthase; Aco, Aconitase; Aho, Acetyl CoA hydrolase; Akgd, Alpha ketoglutarate dehydrogenase; Ato, Acetyl CoA transferase; Cs, Citrate synthase; Frb, Fructose bisphosphatase; Fum, Fumarase; Gpd, Glyceraldehyde-3-phosphate dehydrogenase; Icdh, Isocitrate dehydrogenase; Kar, Ketol-acid reductoisomerase; Mdh, Malate dehydrogenase; Pepc, Phosphoenolpyruvate carboxykinase; Por, Pyruvate ferredoxin oxioreductase; Ppd, Pyruvate phosphate dikinase; Pph, Phosphopyruvate hydratase; Ppk, Phosphoglycerate kinase; Pta, Phosphotransacetylase; Pyc, Pyruvate carboxylase; Sucoas, Succinyl-CoA synthetase; Sudh, Succinyl-CoA dehydrogenase
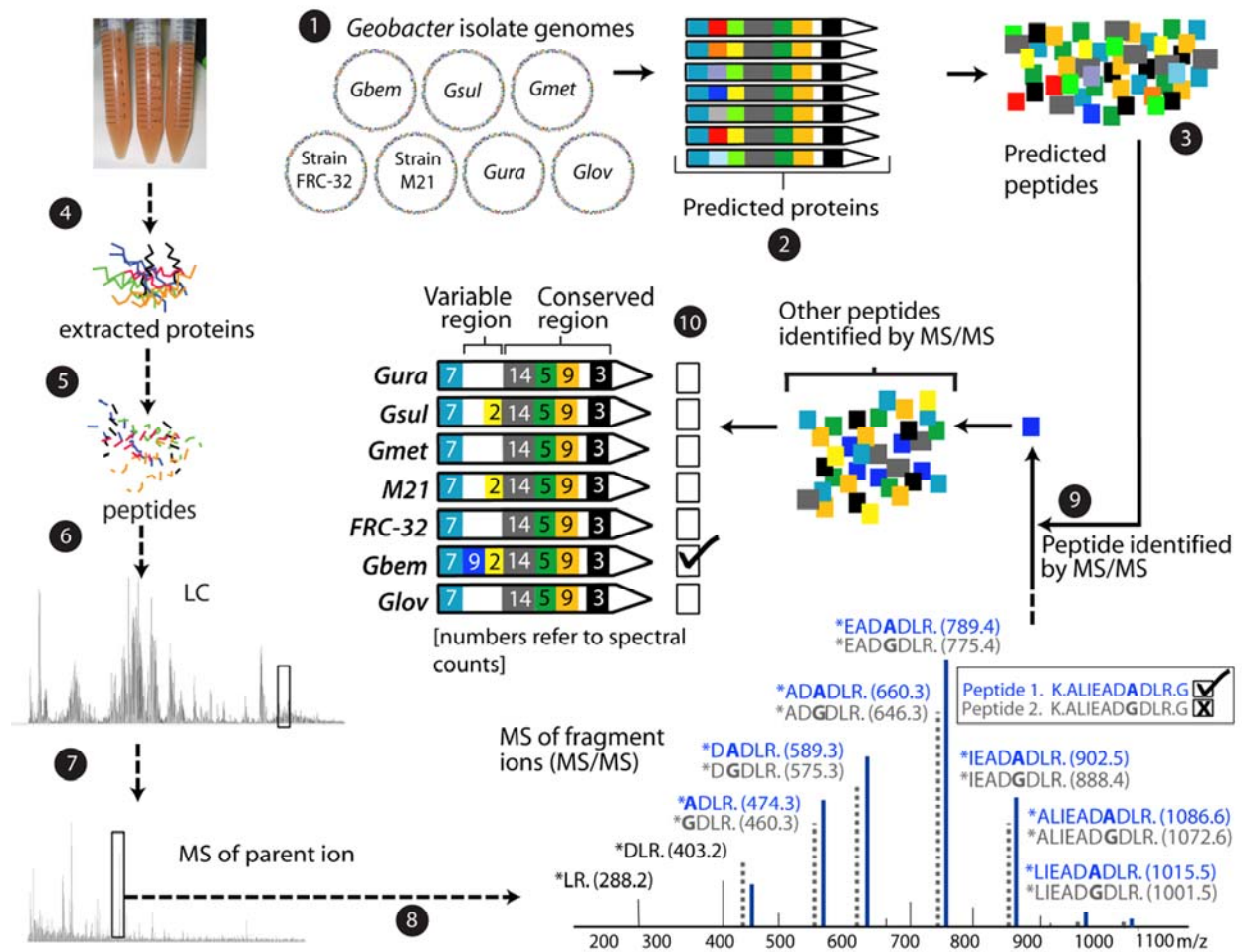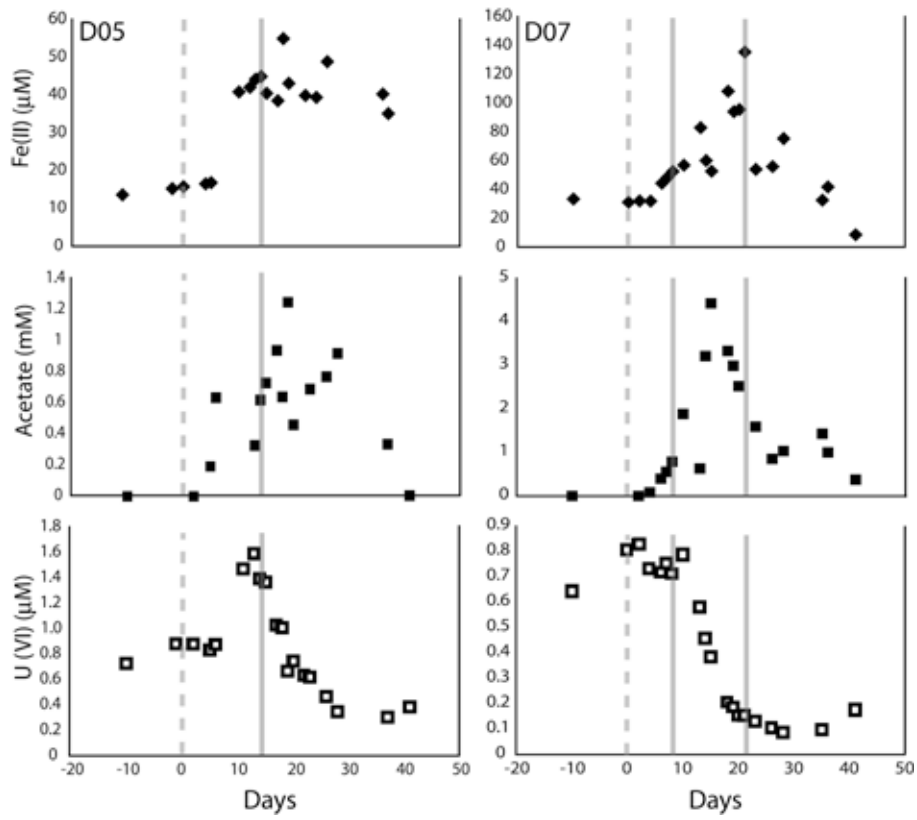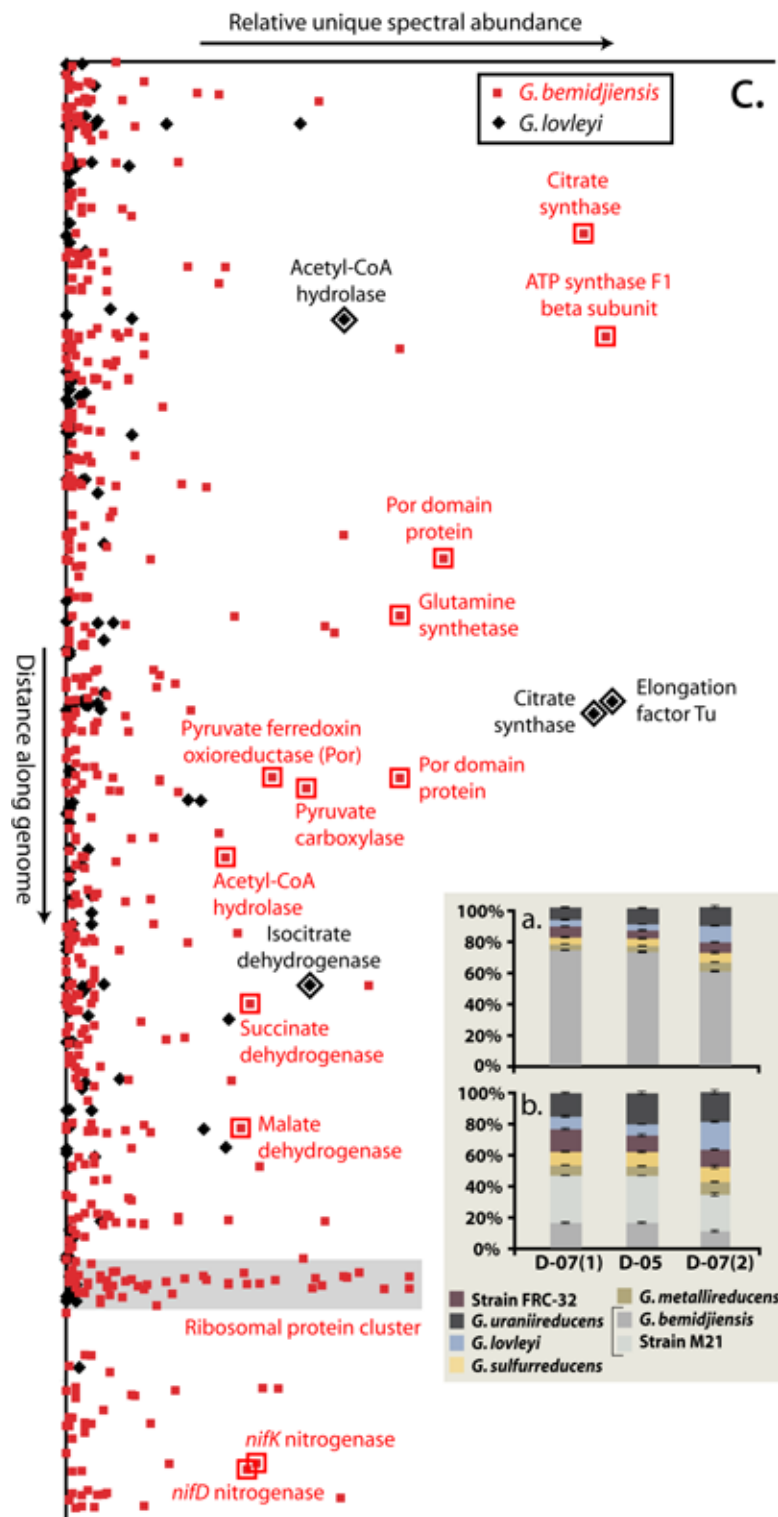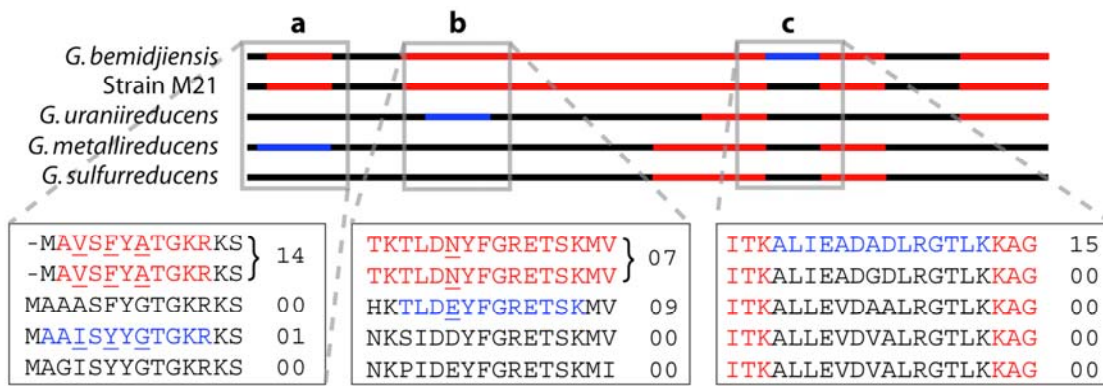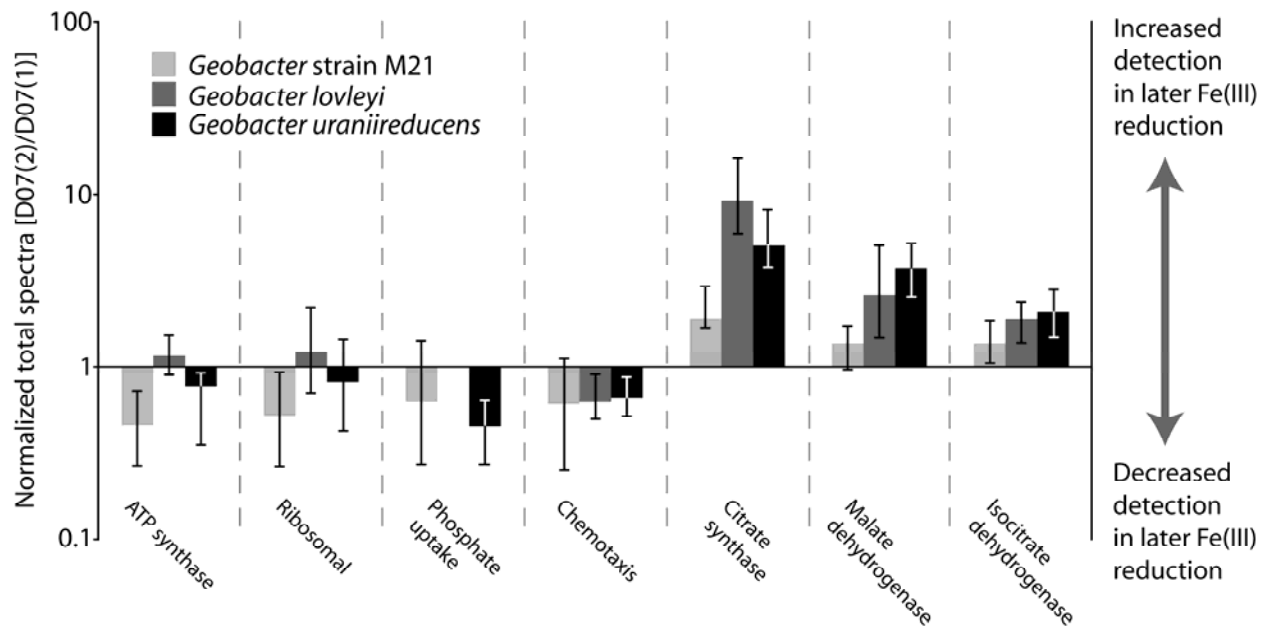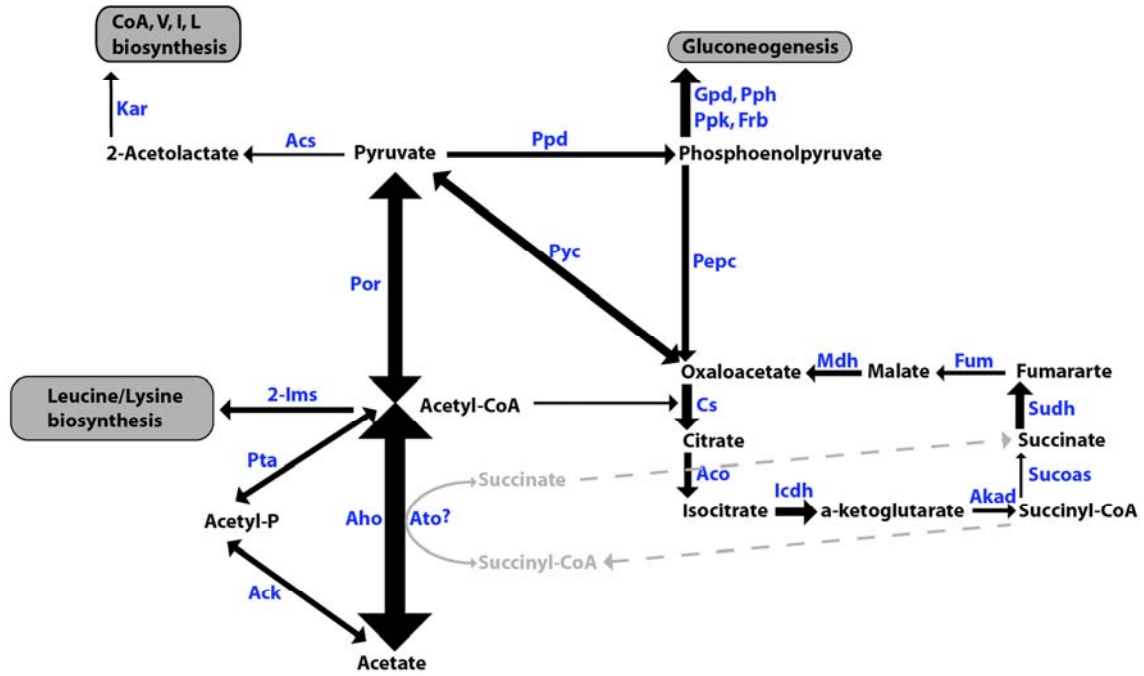
Figure 1.

Figure 2.

Figure 3.

Figure 4.

Figure 5.

Figure 6.